



## Article

# Cu-Doped TiN<sub>x</sub>O<sub>y</sub> Thin Film Resistors DC/RF Performance and Reliability

Lev V. Shanidze<sup>1</sup>, Anton S. Tarasov<sup>1,2</sup> , Mikhail V. Rautskiy<sup>1</sup>, Fyodor V. Zelenov<sup>3</sup>, Stepan O. Konovalov<sup>3</sup>, Ivan V. Nemtsev<sup>1,2</sup> , Alexander S. Voloshin<sup>1,2</sup>, Ivan A. Tarasov<sup>1</sup>, Filipp A. Baron<sup>1,\*</sup> and Nikita V. Volkov<sup>1</sup>

<sup>1</sup> Federal Research Center KSC SB RAS, Kirensky Institute of Physics, 660036 Krasnoyarsk, Russia; shanidze.l.v@mail.ru (L.V.S.); taras@iph.krasn.ru (A.S.T.); rmv@iph.krasn.ru (M.V.R.); ivan\_nemtsev@mail.ru (I.V.N.); avoloshin@sfu-kras.ru (A.S.V.); tia@iph.krasn.ru (I.A.T.); volk@iph.krasn.ru (N.V.V.)

<sup>2</sup> Department of Radio Electronics, Siberian Federal University, 660041 Krasnoyarsk, Russia

<sup>3</sup> Institute of Space Technology, Reshetnev Siberian State University of Science and Technology, 660037 Krasnoyarsk, Russia; fyodor.zelenov@yandex.ru (F.V.Z.); kco.konovalov@yandex.ru (S.O.K.)

\* Correspondence: spintron@hotmail.com

**Featured Application:** High-frequency integrated circuits, heterogeneously integrated and hybrid RF circuits.

**Abstract:** We fabricated Cu-doped TiN<sub>x</sub>O<sub>y</sub> thin film resistors by using atomic layer deposition, optical lithography, dry etching, Ti/Cu/Ti/Au e-beam evaporation and lift-off processes. The results of the measurements of the resistance temperature dependence, non-linearity, S-parameters at 0.01–26 GHz and details of the breakdown mechanism under high-voltage stress are reported. The devices' sheet resistance is  $220 \pm 8 \Omega/\square$  ( $480 \pm 20 \mu\Omega\cdot\text{cm}$ ); intrinsic resistance temperature coefficient (TCR) is  $\sim 400 \text{ ppm}/^\circ\text{C}$  in the T-range of 10–300 K; and S-parameters versus frequency are flat up to 2 GHz with maximum variation of 10% at 26 GHz. The resistors can sustain power and current densities up to  $\sim 5 \text{ kW}\cdot\text{cm}^{-2}$  and  $\sim 2 \text{ MA}\cdot\text{cm}^{-2}$ , above which they switch to high-resistance state with the sheet resistance equal to  $\sim 200 \text{ k}\Omega/\square$  ( $\sim 0.4 \Omega\cdot\text{cm}$ ) caused by nitrogen and copper desorption from TiN<sub>x</sub>O<sub>y</sub> film. The Cu/Ti/TiN<sub>x</sub>O<sub>y</sub> contact is prone to ageing due to gradual titanium oxidation while the TiN<sub>x</sub>O<sub>y</sub> resistor body is stable. The resistors have strong potential for applications in high-frequency integrated and hybrid circuits that require small-footprint, medium-range resistors of 0.05–10 k $\Omega$ , with small TCR and high-power handling capability.

**Keywords:** high-frequency passive components; high power density; thin film; copper doped titanium oxynitride; non-linear; resistors; heterogeneous integration



**Citation:** Shanidze, L.V.; Tarasov, A.S.; Rautskiy, M.V.; Zelenov, F.V.; Konovalov, S.O.; Nemtsev, I.V.; Voloshin, A.S.; Tarasov, I.A.; Baron, F.A.; Volkov, N.V. Cu-Doped TiN<sub>x</sub>O<sub>y</sub> Thin Film Resistors DC/RF Performance and Reliability. *Appl. Sci.* **2021**, *11*, 7498. <https://doi.org/10.3390/app11167498>

Academic Editor: Valentina Belova

Received: 7 July 2021

Accepted: 13 August 2021

Published: 16 August 2021

**Publisher's Note:** MDPI stays neutral with regard to jurisdictional claims in published maps and institutional affiliations.



**Copyright:** © 2021 by the authors. Licensee MDPI, Basel, Switzerland. This article is an open access article distributed under the terms and conditions of the Creative Commons Attribution (CC BY) license (<https://creativecommons.org/licenses/by/4.0/>).

## 1. Introduction

There is a steady technology trend in wireless communications towards the system-on-chip (SoC) solutions [1–3]. However, it is not always easy to realize high performance RF analog and digital circuits on a single silicon chip due to the Si CMOS device performance limitations at RF frequencies. At the same time, wide-band gap semiconductors (GaN, AlGaN, SiC and GaO) and low loss dielectric (Al<sub>2</sub>O<sub>3</sub>, MgTiO<sub>3</sub>, SrTiO<sub>3</sub>, MgO and SiO<sub>2</sub>) substrates offer performances superior to silicon for implementing active and passive RF circuits. However, direct integration of GaN on silicon is still challenging [4,5] and not all wireless products require SoC integration with digital circuits. In order to lower the cost and shorten the time to market, RF system designers of niche applications usually favor cheap, simple and flexible technology such as heterogeneous integration of discrete RF components on a low cost board material such as RO4000<sup>®</sup> (Rogers Corporation, Chandler, AZ, USA). Recently, however, an alternative integration technology of RF components emerged, with passive components integrated directly on the wafer or board by the thin

film technologies and active components placed using the surface mounting technique [6]. The high potential of this new hybrid technology is in its relatively low cost, small circuit footprint, ease in combining different materials and components, flexibility in the choice of substrate and enhanced yield and frequency band-width. All of these factors considerably expand the circuit physical parameters' design space and allows the designer to better optimize the circuit performance. Titanium oxynitride ( $\text{TiN}_x\text{O}_y$ ) thin film is a potential material candidate for resistors in such technology since it provides low temperature coefficient of resistance (TCR), high resistivity, high power handling capability, ease of process integration with other thin film components and was successfully tested in similar integration technology using reactive dc magnetron sputtering [7].

Recently, we have demonstrated a simple innovative ALD technology growth technique of Cu-doped  $\text{TiN}_x\text{O}_y$  thin film with high uniformity that is suitable for further device fabrication [8]. We believe that this technology is a highly promising route to develop the  $\text{TiN}_x\text{O}_y$  resistors for industrial applications. This paper reports the measurements results of the  $\text{TiN}_x\text{O}_y$  thin film resistors TCR, nonlinearity in extended temperature range from 10 to 400 K, S-parameters at RF, high-power handling capability, performance as fusible resistors and aging effects. A simplified compact model of the resistors is extracted from simulations matched to the S-parameters' high-frequency measurements.

## 2. Materials and Methods

Thin Cu-doped  $\text{TiN}_x\text{O}_y$  films ( $x \sim 0.82$ ,  $y \sim 1.43$ ) was fabricated using the atomic layer deposition (ALD) and fully characterized by standard experimental techniques, which revealed the films' structure, chemical composition, optical and transport properties and are reported elsewhere [8].  $\text{TiCl}_4$  liquid precursor,  $\text{NH}_3$  gas, background  $\text{O}_2$  and background Cu-atoms were used as the input components for the growth process performed in the Picosun SUNALE™ (Picosun Oy, Masala, Finland) R-200 ADVANCED reactor at 420 °C. There were two groups of samples: G1 lightly-(or unintentionally) Cu-doped and G2 highly-(or intentionally) Cu-doped. In both cases, the Cu-atoms were brought into the ALD chamber by forming gas. The likely source of the copper impurities was the forming gas tank brass outlet. However, the reactor chamber was passivated with 100–120 nm  $\text{Al}_2\text{O}_3$  prior to loading and growing the G1-samples, while the G2-samples were grown right after the exposure to the Cu-carrying forming gas, i.e., without  $\text{Al}_2\text{O}_3$  passivation of the ALD reactor.

Resistors studied in this work were formed from the lightly Cu-doped  $\text{TiN}_x\text{O}_y$  films (G1-samples) [8] that were grown on a mirror finished 500  $\mu\text{m}$  thick CT-32-1 Sitall (SIT) wafer, which is a Mg-doped, quartz-like polycrystalline ceramic with dielectric constant 9.7–10 and loss tangent of 0.0005 (at 10 GHz). The  $\text{TiN}_x\text{O}_y$  resistor active area (body) was defined by optical lithography followed by plasma etching in RIE-1701 Nordson MARCH using a gas mixture of  $\text{CF}_4$  (15 sccm)/ $\text{O}_2$  (3 sccm) at 250 W RF power and 250 mTorr pressure for 2 min. The resistors' electric contacts were formed as the second layer metallization by aligned optical lithography using negative photoresist AZ nLOF 2035 and e-beam evaporation of Ti (5 nm)/Cu (1  $\mu\text{m}$ )/Ti (5 nm)/Au (50 nm), followed by lift-off. We fabricated two groups of resistors: short (1-square, 30  $\times$  30  $\mu\text{m}$ ) and long (3-square long, 90  $\times$  30  $\mu\text{m}$ ), with the same geometry of the routing and pads. The layout shown in Figure 1 was designed for both DC and high-frequency measurements. Source Meter 2634b (Keithley Instruments, LLC, Solon, OH, USA) connected to the EMPX-HF (Lake Shore Cryotronics, Westerville, OH, USA) probe station was used for DC resistance measurements at quasi-stationary varied temperatures 10–300 K.

The resistors' morphology and EDX spectra for Mg, Al, Ti, Cu, O and N were investigated by using TM4000 Plus (Hitachi, Japan) in the BSE mode with an acceleration voltage of 20 kV equipped with an EDX XFlash Detector 630 Hc (Bruker, Germany). The sample was mounted with a carbon conductive double coated SEM adhesive on a SEM sample stub. Since no metal coating was applied to the sample surface prior to taking the SEM measurements, the surface charging occurred despite using the charge suppression scan

mode of the SEM. In order to investigate the chemical composition of the specimens and the uniformity of the distribution of elements over the surface, the above listed elements mapping was performed over the resistor body, contacts and surrounding area, and they were visualized and quantified by using the Quantax 70 (Bruker, Billerica, MA, USA) software. The acquisition time was 5 min for all samples.

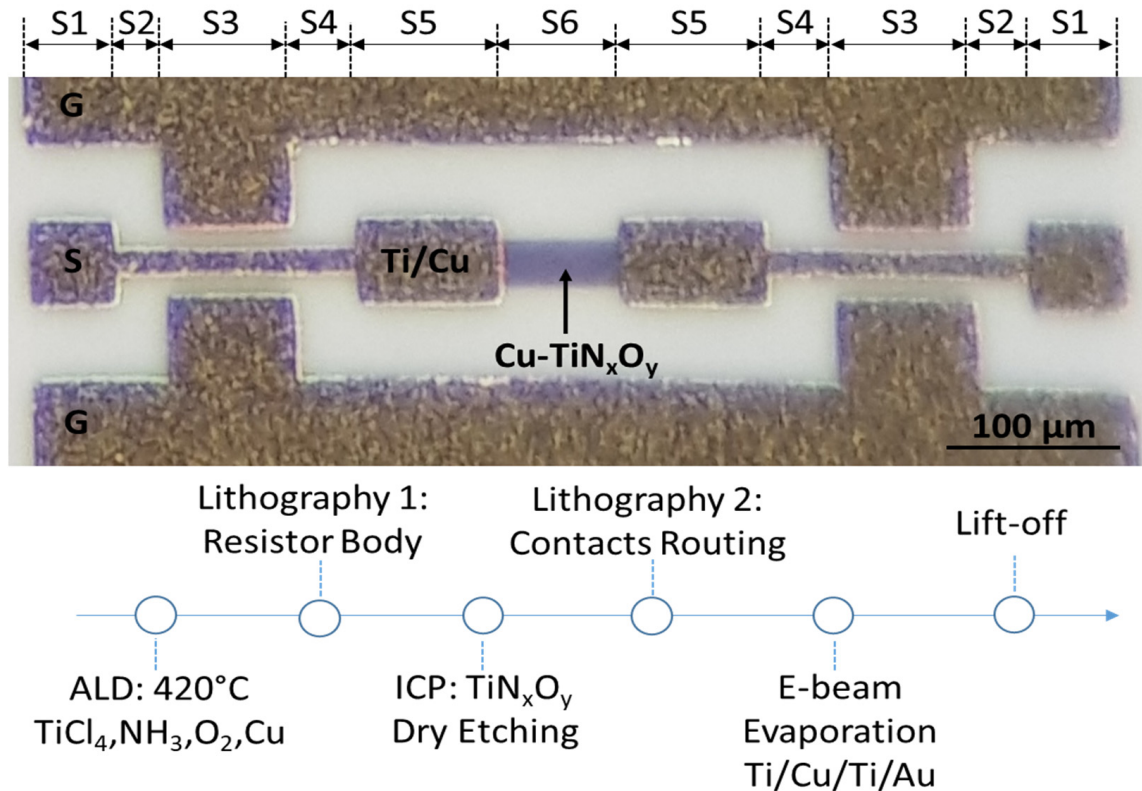


**Figure 1.** RF resistor fabricated from 22 nm thick Cu-doped  $\text{TiN}_x\text{O}_y$  film grown by ALD. The resistor body is connected to ground-source-ground (GSG) copper routing designed for DC/RF measurements. Titanium was used as the copper adhesion layer. The structure is schematically broken into S1–S6 sections for high-frequency modeling. The fabrication process flow diagram is shown below the resistor image.

We investigated the  $\text{Cu-TiN}_x\text{O}_y$  resistors high-frequency transmission properties by measuring their S-parameters at 0.01–26 GHz using the ZNB (Rohde & Schwarz, Munich, Germany) vector analyzer and MPI TS150 (MPI Corporation, Taiwan) probe station. The numerical simulations of the copper routing structure high-frequency behavior were performed by using the CST Microwave Studio environment. We used a simple model of resistor and capacitor connected in parallel to model the  $\text{Cu-TiN}_x\text{O}_y$  resistor body and fit theoretical curves to the experimental data for S-parameters.

### 3. Results

The DC measurements of the  $\text{Cu-TiN}_x\text{O}_y$  film sheet resistance produced a value of  $220 \pm 8 \Omega/\square$ , the resistor thickness extracted from TEM data was  $22 \pm 1 \text{ nm}$ , and its effective resistivity was  $480 \pm 20 \mu\Omega\cdot\text{cm}$ . In order to explore the stability of resistors, we measured their T-dependence in two sets of measurements separated by 18 months. Shown in Figure 2 is the temperature dependence of the extrinsic (total),  $\text{Cu-TiN}_x\text{O}_y$  sheet ( $R_{SH}$ ) and  $\text{TiN}_x\text{O}_y/\text{Ti/Cu}$  contact ( $R_C$ ) resistances extracted from the extrinsic values using the following expressions:

$$\begin{cases} R_{SH} = (R_{3sq} - R_{1sq})/2 \\ R_C = (3 \cdot R_{1sq} - R_{3sq})/4 \end{cases} \quad (1)$$

where  $R_{1sq}$  and  $R_{3sq}$  are the measured extrinsic resistances of 1-square and 3-square long resistors.

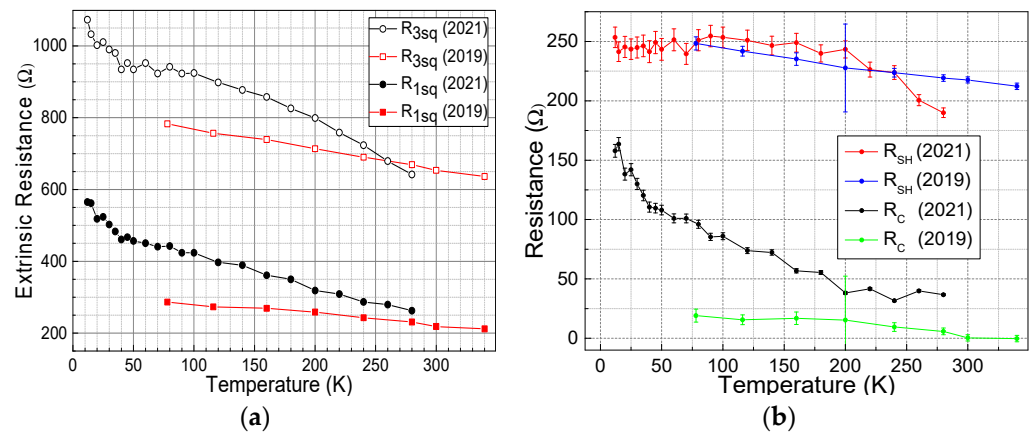


**Figure 2.** Two sets of the Cu-TiN<sub>x</sub>O<sub>y</sub> thin film resistors  $R(T)$  measurements taken 18 months apart in the year 2019 and 2021, accordingly. The width/thickness is 30  $\mu\text{m}$ /22 nm, and the lengths are 30  $\mu\text{m}$  and 90  $\mu\text{m}$  for the 1-square and 3-square resistors, respectively. The resistors are as follows: (a) extrinsic (measured) resistance and (b) extracted Cu-TiN<sub>x</sub>O<sub>y</sub> sheet ( $R_{SH}$ ) and TiN<sub>x</sub>O<sub>y</sub>/Ti/Cu contact ( $R_C$ ) resistances.

The above data suggest there was an ageing effect present in both resistors. Indeed, the measurements in the years 2019 and 2021 revealed that the differential resistance at zero external bias increased by 10–15%. There are several aspects of ageing implied by the data from Figure 2b: the data become noisier, the main contribution to the resistance increase comes from the contacts degradation,  $R(T)$  is strongly non-linear and the sheet resistance of the resistor body becomes essentially flat (within experimental error) below 200 K. However, the contact resistance almost tripled at room temperature and increased up to five times at low temperature due to the ageing.

All  $I$ - $V$  curves of resistors were linear at zero bias, but as the applied voltage increased, the differential resistance decreased. For low-frequency large signal applications, we quantified this non-linearity by introducing the  $U_{10}$  parameter, which was the voltage that caused a 10% decrease in the differential resistance compared to its value at zero bias, as shown in Figure 3a. The non-linearity of  $I$ - $V$  curves was also affected by the ageing phenomena. Figure 3b compares the  $U_{10}$  T-dependence in short and long resistors measured at different times. The non-linearity of resistors has notably increased at low temperatures as the associated parameter  $U_{10}$  has decreased.

More detailed characterizations of resistors' non-linearity including an analytical expression for  $I$ - $V$  dependencies at different temperatures are needed for high-frequency circuits design. Therefore, we fitted the experimental  $I$ - $V$  curves by the following polynomial function where we only kept significant terms:

$$I(V) = B_1V + B_3V^3 + B_5V^5 + B_7V^7 \quad (2)$$

and extracted its coefficients at different temperatures. In the function (2)  $I$  and  $V$  are the current and voltage across the resistor and the coefficient  $B_1$  is the conductivity of the resistor, while the other coefficients do not have simple physical meaning and are rather mathematical entities. The non-linear current polynomial coefficients were calculated for resistors based on  $I$ - $V$  curves measurements, their absolute values are summarized in Figure 4. All coefficients were positive except  $B_5$ , which was strictly negative. The fitting fidelity was high, as evidenced by the adjusted R-square value of 0.99997. The fitting parameters extracted from the non-linear  $I$ - $V$  curve show some differences that seem to increase as temperature decreases. We believe that the origin of these differences is related to the age dependent contact resistance.



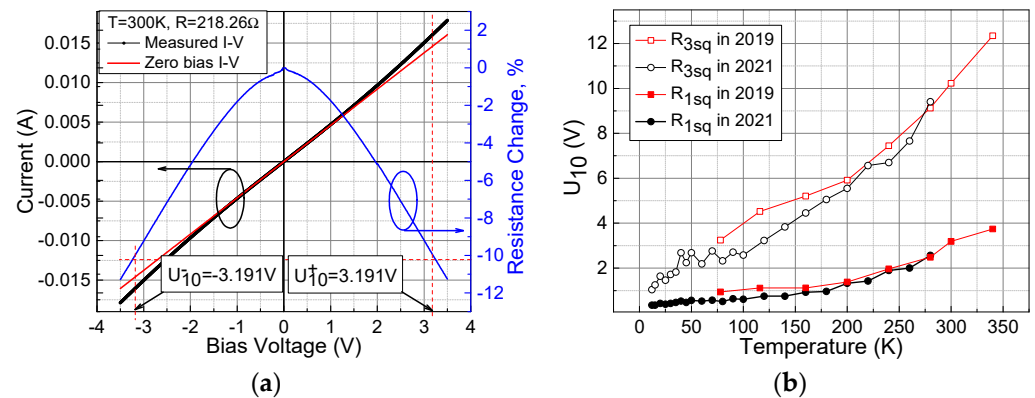


**Figure 3.** Cu-TiN<sub>x</sub>O<sub>y</sub> resistors non-linearity: (a) definition of the non-linearity parameter  $U_{10}$ , which is the voltage that causes the differential resistance 10% change compared to its value at zero bias. In this particular example of I-V curve for 1-square long resistor measured at room temperature,  $U_{10} = 3.191$  V. (b) Resistors non-linearity parameter  $U_{10}$  as a function of temperature measured 18 months apart.

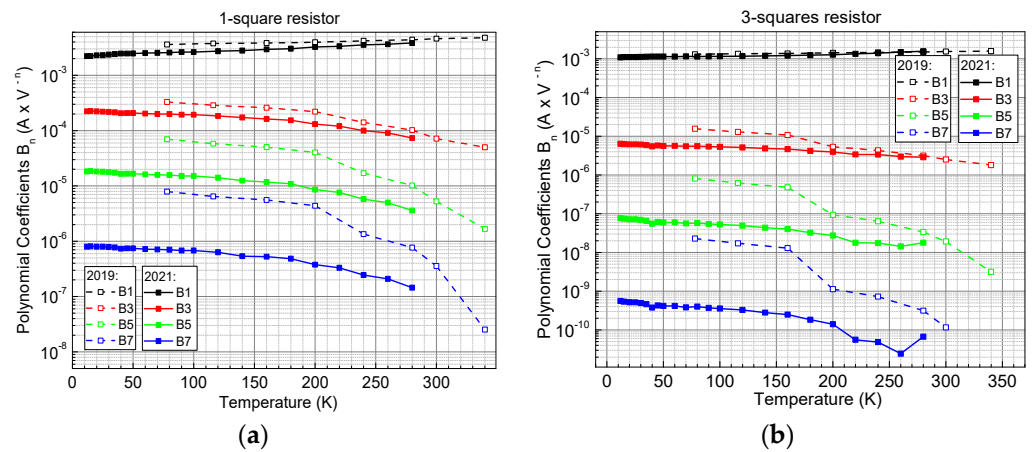


**Figure 4.** T-dependence of the coefficients absolute values for non-linear polynomial fit of experimental  $I-V$  curves for the following: (a) 1-square and (b) 3-square resistors. All coefficients were positive except for  $B_5$ , which was negative.

The current in Cu-doped TiN<sub>x</sub>O<sub>y</sub> resistors increases rather than saturates at higher voltages. This may cause a thermal runaway problem in these resistors when operating in real circuits, so we decided to explore the higher power handling capability of resistors and their maximum power handling capability at higher voltages. Figure 5 shows the results of the slow high-voltage stress test for long resistor with a 15 s bias voltage sweep from zero to maximum voltage. We began with a 11 V voltage cap and gradually increased it to 30 V in four consecutive tests using the same resistor. Continuous visible light emission (inset photos in Figure 5a) was observed for 10–15 s with maximum intensity near 12 V due to the resistor heating followed by a rapid irreversible resistance increase near 24 V in the seventh test. The light emission starts more or less uniformly over the resistor body, but then narrows down to the middle part of the body and then drifts as a focused light source towards the high-bias terminal at higher voltages. After seven high-voltage runs, the resistor ceases to emit light and changes its state to what we call a “burnt” state, characterized by a considerably higher sheet resistance; however, it does not break open even at 30 V and keeps functioning as a non-linear  $\sim 100$  k $\Omega/\square$  resistor.

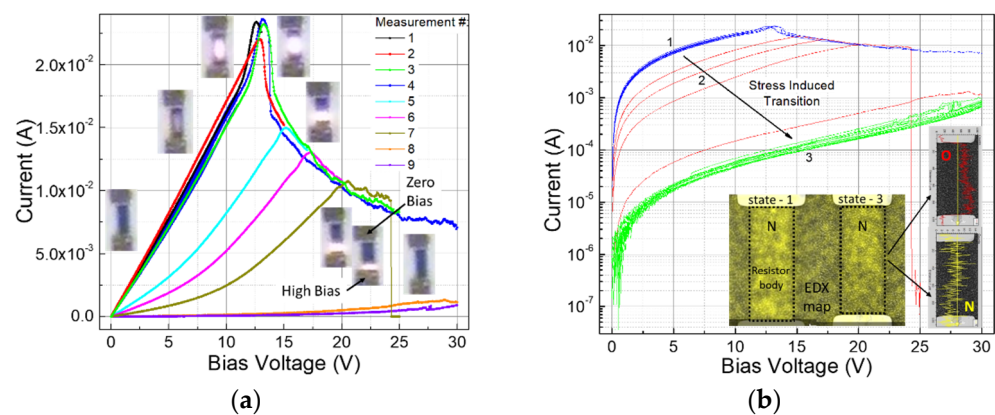


**Figure 5.** High voltage stress burning tests of the 3-square Cu-TiN<sub>x</sub>O<sub>y</sub> thin film resistor: (a) The maximum stress voltage progressively increased from 11 to 30 Volts in nine consecutive measurements (shown in nine different colors); the maximum current peaks of the IV-curves correspond to light emission by resistor body, eventually resulting in irreversible change and the phase transition shown in (b) (red curves of group 2) from low-resistance state (blue curves of group 1) to high-resistance state (green curves of group 3). Shown at the yellow inset of (b) is EDX nitrogen concentration distribution maps for the normal (state-1) and burnt (state-3) resistors, which reveals noticeable N-concentration gradient in the later.

In order to find a physical explanation for the resistive state difference between normal and burnt resistors, we visualized their chemical composition by using the color-coded EDX data. Both working and burnt resistors have all their constituting elements (except for the nitrogen and oxygen) uniformly distributed over the active areas. The inset of Figure 5b shows the EDX data color map of the N-concentration distribution (in yellow) in resistor before (state-1) and after the burning test (state-3), as well as the line scans EDX data for nitrogen and oxygen along the burnt resistor. A noticeable N-gradient can be observed in the burnt resistor, indicating lower x-content in Cu-TiN<sub>x</sub>O<sub>y</sub> towards the high-bias terminal of the resistor. Since Cu-concentrations in both resistors do not exceed 1% and the resistors body is too thin (22 nm), the EDX Cu-signal was too weak to resolve the difference in Cu-concentration between the resistors. However, we believe that copper desorbed from the surface accompanied by the nitrogen depletion during the resistors burning test. Indeed, the remaining finite resistivity after the burning test ( $\sim 0.4 \Omega \cdot \text{cm}$  at 10 V) agrees well with the values for undoped TiN<sub>x</sub>O<sub>y</sub> with similar O-content ( $\sim 1 \Omega \cdot \text{cm}$  at  $y = 45\%$ ) published elsewhere [9]. Since the Cu-doped TiN<sub>x</sub>O<sub>y</sub> resistors are not destroyed completely by high-current but rather continue to function in high-resistivity state, they may be used as integrated fusible resistors in order to limit currents to tens mA range and to provide the benefit of both overcurrent and inrush current protection.

In order to explore the prospects of using the Cu-doped TiN<sub>x</sub>O<sub>y</sub> thin film resistors as fusible resistors, we studied their lifetime as a function of power. For that, we increased the maximum voltage to 200 V and varied the voltage ramp magnitude. Figure 6 shows the stressed resistors  $I$ - $V$  curves family measured for several resistors destroyed at different voltage ramps. As expected, low ramps yield lower maximum current and critical voltage due to a larger time-integral of power, i.e., dissipated energy. These data were used to calculate the fusible resistors life-time versus maximum power shown in Figure 6b. Figure 6c shows micro-images of a resistor burnt by steep high voltage ramp along with its EDX 2D color-coded map of the nitrogen and oxygen concentration distribution. From both the optical image and EDX data, it appears that the fusing action of resistors is, indeed, due to the nitrogen replacement with oxygen, i.e., transition from optically non-transparent N-rich to a transparent O-rich TiN<sub>x</sub>O<sub>y</sub>. This N-to-O transition happens dynamically when increasing the voltage and always starts at a point close to the middle of the resistor body, gradually propagating towards the high-bias terminal with the propagation speed

proportional to the voltage increase rate. The N-to-O transition boundary front propagates by discrete jumps accompanied by the light micro flashes.

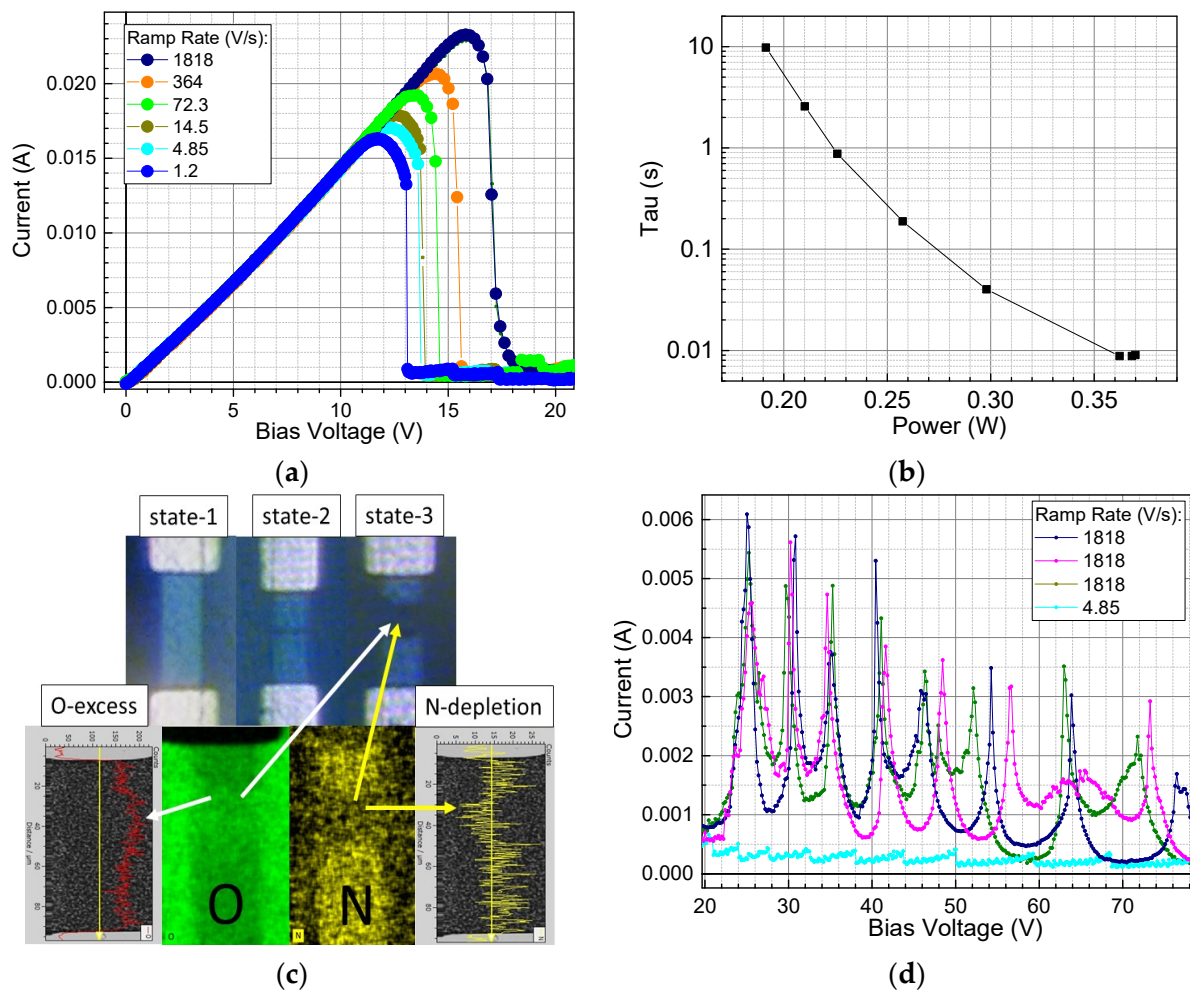


**Figure 6.** High voltage stress test: (a)  $I$ - $V$  curves measured for several resistors destroyed at different voltage ramps, lower ramps fuse resistor at low voltage; (b) fusible resistor life-time versus maximum allowed power in the low-resistivity state; (c) EDX 2D map showing relative oxygen excess and nitrogen depletion in the voltage stress damaged region of the resistor body; and (d) oscillatory current spikes observed at high voltage ramps at higher voltages. The spikes gradually turn into a saw-like pattern as we decreased the voltage ramp from 1818 V/s down to 4.85 V/s.

Figure 6d shows the same  $I$ - $V$  curves as in Figure 6a at higher voltages revealing intriguing features: pronounced current oscillations. The first peak voltage is always fixed at  $\sim 25$  V for all destroyed resistors, and higher peaks gradually diminish and ungroup. These oscillations appeared only at high voltage ramps and the higher the ramp the higher their magnitude and the narrower the peaks. At lower ramps these peaks diminish and start shifting to lower voltages before transforming into almost equidistant saw-like current pattern. The highest voltage current peak appears as a sharp spike measuring 5–10 mA at 100–120 V, and the resistor eventually ( $>150$  V) explodes by sublimating the metal traces to pads if one increases the voltage even further. The current peaks of Figure 6d are related to the light micro flashes mentioned above and are associated with the micro-scale breakdown-like step-by-step conversion of the parts of the resistor body that they spark through from grey to transparent. Half of resistor attached to the terminal at zero voltage always preserves its N-rich composition associated with the grey color.

Shown in Figure 7 are the results of the S-parameters' high-frequency measurements and simulations. In order to build a simple RF circuit model of the resistor, we performed

numerical simulations of the structures using the quasi-2D model consisting of coplanar micro-strip transmission lines (TRL) chain. Each TRL element of the chain represents a section S1–S6 of the copper routing layout shown in Figure 1 with the associated signal line width, length and signal to ground gap. TRL elements do not contain any fitting parameters, and their dimensions are taken from the drawn topology of the resistor layout; thus, their transfer function is fixed. A lumped model of the resistor and capacitor connected in parallel was used to model the Cu-TiN<sub>x</sub>O<sub>y</sub> thin film sheet resistance of the resistor body and terminals AC-coupling. The best matching was achieved with 250 Ω/□ for short and 215 Ω/□ for long resistors, with 15 fF and 5 fF bypass capacitors, respectively.

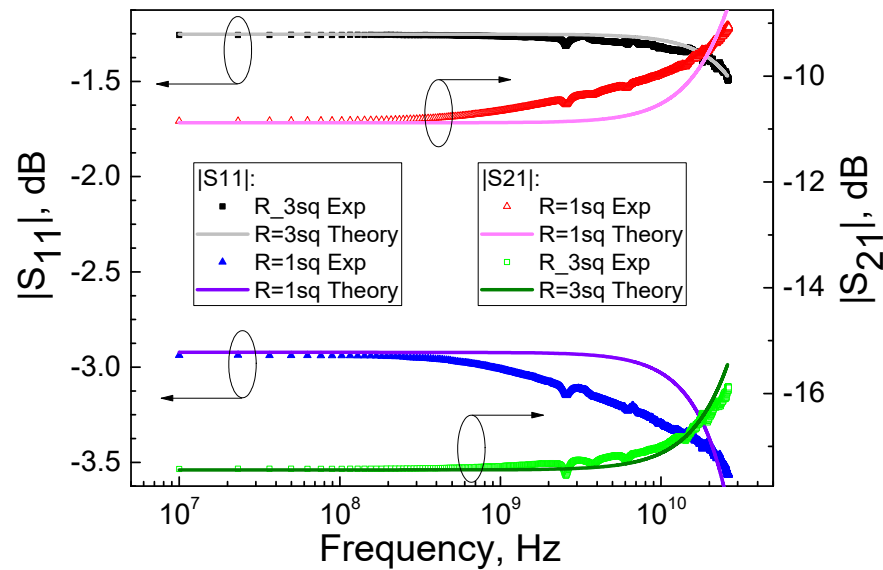


**Figure 7.** Measured two-port S-parameters for the following: 1-square (blue and red) and 3-square (black and green) resistors and their theoretical values were obtained using 2D coplanar micro-strip lines model for copper routing and lumped model of resistor and capacitor connected in parallel (for the Cu-TiN<sub>x</sub>O<sub>y</sub> resistor body). The best matching is achieved with the Cu-TiN<sub>x</sub>O<sub>y</sub> thin film sheet resistance of the following: 250 Ω/□ for 1-square and 215 Ω/□ for 3-square resistors with 15 fF and 5 fF bypass capacitors, respectively. The left and right y-axes correspond to the magnitude of the reflection and transmission coefficients of the RF power.

#### 4. Discussion

We fabricated and measured 1-square and 3-square resistors from the ALD-grown Cu-TiN<sub>x</sub>O<sub>y</sub> film with Au-finished metal traces of the Cu-routing for DC and RF characterization. The DC sheet resistance equals  $220 \pm 8 \Omega/\square$ , and the intrinsic TCR is  $\sim 400 \text{ ppm}/^\circ\text{C}$ , which is comparable to NiCr resistors and almost two orders of magnitude smaller than the values reported for TiN single-crystal films [10]. Compared to the monocrystalline TiN the Cu-TiN<sub>x</sub>O<sub>y</sub> resistance is roughly 20 times higher [11]. However, due to the TiN<sub>x</sub>O<sub>y</sub>/Ti/Cu interface contact reliability issues (ageing), the extrinsic TCR of the resistors became considerably higher over the course of 18 months. Initially the extrinsic R(T) dependence showed only a slight increase at low temperatures; however, this trend increased substantially due to the ageing effect (Figure 2a). A more detailed analysis that separated the resistor body from the contact contribution to the net resistance revealed that the contact resistance increased dramatically and became a non-linear function of temperature after 18 months (Figure 2b). At the same time the intrinsic (resistor physical body) resistance remained stable below 200 K and decreased only slightly above 200 K.

We studied the non-linearity of the resistors and found that it increased as they aged:  $U_{10}$  decreased almost five times at low temperature (Figure 3b). Non-linear polynomial fits of the resistors'  $I$ - $V$  curves measured at different temperatures showed that all significant coefficients of non-linear terms in (2) increased significantly at low temperatures while



the linear term coefficient, i.e., conductance decreased 20% in the early measurements and up to 100% in the latest studies (Figure 4). The non-linear divergence of the contact resistance at low temperature is believed to be due to a  $\text{TiO}_x$  potential barrier gradually formed at the interface between the  $\text{TiN}_x\text{O}_y$  film resistor body and Cu/Ti metallization at the contact areas. It is plausible that the titanium adhesion layer became oxidized over the course of 18 months via the oxygen scavenging (gettering) mechanism from the underlying  $\text{TiN}_x\text{O}_y$  film. Since the non-linearity of  $I$ - $V$  curves significantly increased at low temperatures and the  $R(T)$  itself became increasingly non-linear, we suggest there is an increasing admixture of the tunneling and/or thermionic current components in resistors measured after 18 months, i.e., the contact gradually transforms from Ohmic to  $\text{TiO}_x$ -barrier type. However, the resistors'  $I$ - $V$  curves do not saturate yet, which, for example, would be typical for the back-to-back (B2B) Schottky diodes [12]. Therefore, we believe that the parasitic  $\text{TiO}_x$  potential barrier is leaky. This uncertainty in device performance sets our future work goal of resolving the contact ageing problem by eliminating the Ti/ $\text{TiN}_x\text{O}_y$  interface, as the  $\text{TiN}_x\text{O}_y$  thin film resistor itself seems to be stable and capable of functioning at high-power density.

Indeed, given the values of the maximum current, the voltage at the maximum current (Figure 5) and the resistor body dimensions, one may calculate that such a resistor can sustain power density in the low resistivity state up to  $\sim 5 \text{ kW}\cdot\text{cm}^{-2}$ , with currents in the range of tens of mA corresponding to the effective current densities in excess of  $2 \text{ MA}\cdot\text{cm}^{-2}$ . The enhanced robustness of Cu- $\text{TiN}_x\text{O}_y$  resistors was demonstrated by their ability to survive several 10 s open-air incandescence tests (Figure 6a,b), sustaining up to 100 mW or  $40 \text{ W}\cdot\text{mm}^{-2}$  power for about 10 s. At higher power levels, the resistors switch to high-resistivity state due to the nitrogen/copper desorption and local oxidation (Figure 6c) before eventually breaking open explosively at voltages over 150 V due to the copper routing sublimation. Therefore, these devices may have a strong potential as fusible resistors for tens mA currents.

A peculiar pattern of the N-to-O phase transition in  $\text{TiN}_x\text{O}_y$  resistor body starting from the middle and propagating towards the high-bias terminal (shown in the inset of Figure 6a) may be understood by the copper routing heat removal mechanism. Since copper has much higher thermal conductivity than  $\text{TiN}_x\text{O}_y$  and SiTall, effectively—together with the measurement probes—it serves as a heat sink. Since the middle part of the resistor body is the farthest point from the copper heat sink, it has the highest temperature and N-to-O transition outset from there. Once a tiny N-depleted gap of O-rich semi-insulating  $\text{TiN}_x\text{O}_y$  is formed in the middle of the resistor body (Figure 6c), it is instantly exposed to a high field, which may cause avalanche electric breakdown phenomena in the newly formed O-rich semi-insulating phase micro-regions of  $\text{TiN}_x\text{O}_y$  film and, thus, generate the observed current inrush spikes (Figure 6d). The light emission may originate from localized heating or hot electron-hole radiative recombination as well. Indeed, an interesting reproducible oscillatory current spiking behavior has been found at substantially high overvoltage ramps and high voltages. Judging by the associated abrupt changes of color from grey to transparent and the localized microscopic light-flashes synchronized with the observed current spikes, we believe that these current spikes should be related to the high-field avalanche currents and localized phase transition from the high-conductance semi-metallic state of Cu-doped N-rich composition to the low-conductance semi-insulating state of O-rich composition of  $\text{TiN}_x\text{O}_y$  film.

The high frequency S-parameters' data showed relatively low mismatch of resistors across the wafer, which was 0.1% at 10 MHz and gradually increased to 10% at 26 GHz. The simulated S-parameters reproduce the experimental data for long resistors and were slightly off for the short ones at frequencies over 1 GHz (Figure 7). This effect may be due to the increased fringe fields between the resistor body contacts, which are much closer to one another in the short resistor. Full 3D EM simulations are planned in the future in order to account for this mismatch, as the fringe fields' effects may play a significant role in smaller structures, and EM resonances may appear in larger structures. Both effects are

not captured by the cascaded chain of the quasi-2D coplanar lines approximation. Thus, a somewhat higher sheet resistance value of  $250 \Omega/\square$  extracted from the simulations of the short resistor is likely an overestimate due to oversimplified consideration of the fringe fields in simulations. The sheet resistance of  $215 \Omega/\square$  extracted from simulations of the long resistor matched well with the experimental DC value due to reduced AC-coupling of the farther separated terminals in the case of the long resistor. Indeed, the effective bypass capacitors accounting for the terminals' AC-coupling have been extracted to be 5 fF and 15 fF for the long and short resistors, respectively. The S-parameters phase was measured and matched well with simulations in order to yield strictly negative values for all tests, except for the short resistor that in measurements showed slightly positive phase ( $<10^\circ$ ) below 1 GHz. However, the phase never reached  $-90^\circ$ , and the resistor routing structure remained below its self-resonant frequency within the entire frequency band studied in both simulations and experiment. We believe this makes the long resistors structure considered in this work suitable and promising for high-frequency applications of at least up to 26 GHz, effectively rendering them RF resistors.

Overall, our results show satisfactory performance of the Cu-TiN<sub>x</sub>O<sub>y</sub> thin film resistors at elevated power densities and high frequencies. We believe that improved TCR, satisfactory high-frequency matching, high sheet resistance, small footprint, high power-handling capability, the fusibility feature and ease of integration with the standard CMOS BEOL process [13] render the Cu-TiN<sub>x</sub>O<sub>y</sub> thin film resistors a competitive alternative to the pure TiN and NiCr resistors for applications in integrated/hybrid and high-frequency/power circuits.

**Author Contributions:** Formal analysis and project administration, A.S.T.; methodology and devices fabrication, S.O.K.; TiN<sub>x</sub>O<sub>y</sub> thin films growth and characterization, F.V.Z.; electrical transport properties measurements and visualization, L.V.S.; resources allocation and data curation, M.V.R.; electron microscopy and EDX measurements, I.V.N.; simulations and compact modeling, A.S.V.; optical imaging and data analysis, I.A.T.; writing—original draft preparation, conceptualization and executive supervision, F.A.B.; funding acquisition and writing—review and editing, N.V.V. All authors have read and agreed to the published version of the manuscript.

**Funding:** This research was funded by RFBR, Krasnoyarsk Territory and Krasnoyarsk Regional Fund of Science, project code 20-42-240013 and by Grant of the Government of the Russian Federation for Creation of World Tier Laboratories (contract No. 075-15-2019-1886).

**Institutional Review Board Statement:** Not applicable.

**Informed Consent Statement:** Not applicable.

**Data Availability Statement:** Not applicable.

**Acknowledgments:** We would like to acknowledge Andrey A. Leksikov, Konstantin V. Lemberg, Alexey M. Serzhantov and Yaroslav F. Bal'va for the support with RF modelling and measurements of TiN<sub>x</sub>O<sub>y</sub> resistors and Albert N. Masyugin, Anton B. Ivanov, Alexander V. Strezh for the support with processing and fabrication of the devices in Class 1000 clean rooms facility of the Krasnoyarsk Territorial Shared Resource Center, Krasnoyarsk Scientific Center and Russian Academy of Sciences and Krasnoyarsk Regional Center of Research Equipment of the Federal Research Center "Krasnoyarsk Science Center SB RAS" for providing access to high-frequency measurements setup.

**Conflicts of Interest:** The authors declare no conflict of interest.

## References

1. Scholten, C.A. System-on-a-Chip: What Industry Needs to Do. *Solid State Technol.* **2000**, *43*, 121–123.
2. Furber, S.; Bainbridge, J. Future trends in SoC interconnect. In Proceedings of the 2005 International Symposium on System-on-Chip, Tampere, Finland, 17 November 2005; pp. 183–186.
3. Chen, Y.-K.; Kung, S.Y. Trend and Challenge on System-on-a-Chip Designs. *J. Signal Process. Syst.* **2008**, *53*, 246–257. [[CrossRef](#)]
4. Marcon, D.; De Jaeger, B.; Halder, S.; Vranckx, N.; Mannaert, G.; Van Hove, M.; Decoutere, S. Manufacturing challenges of GaN-on-Si HEMTs in a 200 mm CMOS fab. *IEEE Trans. Semicond. Manuf.* **2013**, *26*, 361–367. [[CrossRef](#)]
5. Boles, T. GaN-on-silicon present challenges and future opportunities. In Proceedings of the 12th European Microwave Integrated Circuits Conference (EuMIC), Nuremberg, Germany, 8–10 October 2017; pp. 21–24.

6. Dalmia, S.; Nahalingam, K.; Vijayakumar, S.; Talebbeydokhti, P. A Zero Height Small Size Low Cost RF Interconnect Substrate Technology for RF Front Ends For, M.2 Modules And SiP. In Proceedings of the IEEE 69th Electronic Components and Technology Conference (ECTC), Las Vegas, NV, USA, 28–31 May 2019; pp. 1666–1671. [[CrossRef](#)]
7. Cuong, N.D.; Kim, D.J.; Kang, B.D.; Yoon, S.G.J. Structural and Electrical Properties of  $\text{TiN}_x\text{O}_y$  Thin-Film Resistors for 30 dB Applications of  $\pi$ -type Attenuator. *Electrochem. Soc.* **2006**, *153*, G856–G859. [[CrossRef](#)]
8. Baron, F.A.; Mikhlin, Y.L.; Molokeev, M.S.; Rautskiy, M.V.; Tarasov, I.A.; Volochaev, M.N.; Shanidze, L.V.; Lukyanenko, A.V.; Smolyarova, T.E.; Konovalov, S.O.; et al. Structural, Optical, and Electronic Properties of Cu-Doped  $\text{TiN}_x\text{O}_y$  Grown by Ammonothermal Atomic Layer Deposition. *ACS Appl. Mater. Interfaces* **2021**, *13*, 32531–32541. [[CrossRef](#)] [[PubMed](#)]
9. Yang, X.; Lin, Y.; Liu, J.; Liu, W.; Bi, Q.; Song, X.; Kang, J.; Xu, F.; Xu, L.; Hedhili, M.N.; et al. Highly Conductive Titanium Oxynitride Electron-Selective Contact for Efficient Photovoltaic Devices. *Adv. Mater.* **2020**, *32*, 2002608. [[CrossRef](#)] [[PubMed](#)]
10. Johansson, B.O.; Sundgren, J.-E.; Greene, J.E. Growth and Properties of Single Crystal TiN Films Deposited by Reactive Magnetron Sputtering. *J. Vac. Sci. Technol. A* **1985**, *3*, 303–307. [[CrossRef](#)]
11. Narayan, J.; Tiwari, P.; Chen, X.; Singh, J.; Chowdhury, R.; Zheleva, T. Epitaxial Growth of TiN Films on (100) Silicon Substrates by Laser Physical Vapor Deposition. *Appl. Phys. Lett.* **1992**, *61*, 1290–1292. [[CrossRef](#)]
12. Tang, X.-L.; Zhang, H.-W.; Su, H.; Zhong, Z.-Y. A novel spin-polarized transport effect based on double-Schottky barriers. *Phys. E* **2006**, *31*, 103–106. [[CrossRef](#)]
13. Musschoot, J.; Xie, Q.; Deduytsche, D.; Van der Berghe, S.; Van Meirhaeghe, R.L.; Detavernier, C. Atomic Layer Deposition of Titanium Nitride from TDMAT Precursor. *Microelectron. Eng.* **2009**, *86*, 72–77. [[CrossRef](#)]